

Laser-Driven Micro-Pinch: A Pathway to Ultra-Intense Neutrons*

Putong Wang,^{1,2} Xuesong Geng,³ Guoqiang Zhang,^{4,1,†} Liangliang Ji,^{3,‡} and Yu-Gang Ma^{5,§}

¹Shanghai Institute of Applied Physics, Chinese Academy of Sciences, Shanghai 201800, China

²University of Chinese Academy of Sciences, Beijing 100049, China

³Laboratory of Optical Physics, Institute of Physics, Chinese Academy of Sciences, Beijing 100190, China

⁴Shanghai Advanced Research Institute, Chinese Academy of Sciences, Shanghai 201210, China

⁵Key Laboratory of Nuclear Physics and Ion-Beam Application (MOE),
Institute of Modern Physics, Fudan University, Shanghai 200433, China

Utilizing the laser-driven Z-pinch effect, we propose an approach to generate ultra-short intense MeV neutron source of femtosecond pulse duration. The self-generated magnetic field driven by a petawatt-class laser pulse compresses deuterium in a single nanowire to over 120 times of its initial density, achieving an unprecedented particle number density of 10^{25} cm^{-3} . Through full dimensional kinetic simulations including nuclear reactions, we find these Z-pinchs have the capacity to generate neutron pulses of high intensity and short duration, with a peak flux reaching $10^{27} \text{ cm}^{-2} \text{ s}^{-1}$. Such laser-driven neutron sources are beyond the capability of existing approaches and paves the way for groundbreaking applications in r-process nucleosynthesis studies and high precision Time-of-Flight neutron data measurement.

Keywords: nanowire target, Z-pinch, D-D fusion reaction, laser-plasma, neutron source

I. INTRODUCTION

Conventional neutron sources, spanning isotope, accelerator, and reactor types, have played a pivotal role in advancing diverse scientific and technological domains, including materials science and nuclear physics[1]. Spallation neutron sources, representing the forefront of this evolution, are distinguished as a novel generation of high-intensity, pulsed neutron sources. They achieve neutron flux levels near $10^{17} \text{ cm}^{-2} \cdot \text{s}^{-1}$ with brief pulse widths. These attributes significantly enhance precision in Time-of-Flight (TOF) measurements, a cornerstone in nuclear reactor design and nuclear astrophysics [2, 3].

Despite these advancements, the replication of high neutron flux conditions, which is crucial for understanding r-process nucleosynthesis[4], remains a formidable challenge. Integral to the cosmic formation of heavy elements, neutron star mergers is the primary site for this process[5], while the possibility of the contribution from supernovae explosions is still under debate[6]. These astrophysical events require conditions, including the intensive neutron flux ranging from 10^{22} to $10^{28} \text{ cm}^{-2} \cdot \text{s}^{-1}$, a range still elusive in laboratory settings. This gap not only hinders our comprehensive understanding of these astrophysical phenomena but also limits advancements in related fields such as nuclear physics and astrophysics. The urgency to develop new methodologies capable of achieving these extreme conditions in a controlled

environment is therefore paramount.

The recent development of laser-driven high-intensity neutron sources show the potential to fill this gap due to their exceptional temporal resolution and ability to achieve highly localized neutron beams (spatial resolution) [7, 8]. These sources employ various methodologies, including photoneutron production[9, 10] ($10^{21} \text{ cm}^{-2} \cdot \text{s}^{-1}$), target normal sheath acceleration (TNSA) [11, 12] ($10^{24} \text{ cm}^{-2} \cdot \text{s}^{-1}$), target compression via spherical shells (NIF)[13] ($10^{30} \text{ cm}^{-2} \cdot \text{s}^{-1}$). While these methods offer advancements, the neutron flux from the laser-driven Z-pinch shows the potential to surpass the current capabilities.

Z-pinch is a phenomenon where an axial current flowing through a plasma generates a magnetic field. The interaction between this magnetic field and the current creates a radial Lorentz force, which compresses the plasma radially to a small volume[14]. Fusion and x-ray researches are exploring the potential of Z-pinch devices[15–18]. Recent strides have pivoted around the augmentation of laser-driven Z-pinch mechanics from nanowire arrays[19–21], presenting notable intrigue. These nanowire arrays efficiently absorb the energy from a femtosecond petawatt laser, resulting in a high degree of ionization and intense x-ray generation[22, 23]. Additionally, ions in the array are accelerated, triggering micro-scale fusion reactions[24].

Therefore, we carried out a PIC simulation then find that a fs Petawatt laser can pinch a single nanowire to over 120 times its original density. This ultra-high density achieved through the pinch is referred to as a micro-pinch due to its tiny spatial scale and short duration. Simulations suggest that such micro-pinchs can facilitate nuclear fusion reactions, leading to an intense, short-lived neutron pulse with a unprecedented flux level, $10^{27} \text{ cm}^{-2} \text{ s}^{-1}$.

* This work was supported by the Strategic Priority Research Program of the CAS (No. XDB16), the National Key R&D Program of China (2022YFA1602200, 2022YFA1602400), and the National Natural Science Foundation of China (No. 12235003).

† Corresponding author.

E-mail addresses: zhangguoqiang@sari.ac.cn

‡ Corresponding author.

E-mail addresses: jill@siom.ac.cn

§ Corresponding author.

E-mail addresses: mayugang@fudan.edu.cn

II. SIMULATION SETTING

To investigate the neutron generation process in a Z-pinch setup, we employ full dimensional kinetic simulations to reveal the ultra-short pinch process and the generation of neutrons using the Particle-in-Cell (PIC) code Smilei[25] code. The original nuclear reaction scheme [26, 27] has been introduced in Smilei. Specifically, the cross section for reaction $D + D \rightarrow n + {}^3\text{He}$, has been integrated into the debugging version of Smilei. We have improved the debugging version, corrected and checked the nuclear reaction cross sections, using a periodic boundary condition in a box[28]. In addition, we have also added the nuclear reaction $D + T \rightarrow n + {}^4\text{He}$ (data from [29]) in this paper to see the potential for the higher intensive neutron source.

In our simulation, the nanowire where Z-pinch is triggered is composed of deuterated polyethylene (CD_2). The particle number density of deuterium is set to $\rho = 7.8 \times 10^{22} \text{ cm}^{-3}$. Diameters of 300 nm and 500 nm have been considered with varying wire length. The initial temperature of the particles is set at 300 Kelvin. The nanowire-target is irradiated by 400 nm wavelength circularly-polarized (CP) laser pulses of 30 fs or 60 fs FWHM duration. The dimensionless amplitude of the laser field is ranging $a_0 = 10 - 40$ ($a_0 = eE/m_e c\omega$), here e and m_e are the electron charge and mass, E is the laser electric field, ω is the laser frequency and c is the speed of light in vacuum, respectively. The focal spot size of laser should be big enough to cover the whole single nanowire. A typical focal spot size is about $5 \mu\text{m}$, reaching a peak intensity $\sim 5 \times 10^{21} \text{ W/cm}^2$ ($a_0 = 17$). To avoid numerical heating, the size and the number of cell are adjusted dynamically, according to the volume of the nanowires. One typical cell size is set as $7.5 \text{ nm} \times 5 \text{ nm} \times 5 \text{ nm}$, with 27 macro-particles per cell. There are $640 \times 192 \times 192$ cells for small-sized nanowire, corresponding to a cube $4.8 \mu\text{m} \times 0.96 \mu\text{m} \times 0.96 \mu\text{m}$, which is large enough to hold the whole nanowire in. The simulation boundaries are set to open conditions for both the fields and the particles. Since the field ionization is the dominating ionization process compared with that from Coulomb collisions between particles, to save simulation time, collisional ionization is switched off. The binary collision between deuterium (tritium) is set and nuclear reaction may occur.

III. SIMULATION RESULT

When irradiated by the ultrashort, high-intensity laser pulses, the atoms inside the wire undergo field ionization. The ionization process leads to a considerable potential difference on the surface of nanowire. This potential disparity is balanced by a significant return current flowing across the nanowire's surface, maintaining quasi-neutrality. For a rough estimation, we assume electrons ionized from atoms within the nanowire are mostly distracted by the laser, corresponding to total charge of $Q = 1.3 \times 10^{-8} \text{ C}$. The current can be calculated as $I = Q/t$, where t represents the FWHM duration of the laser, set at 60 fs. This estimated current of $2.2 \times 10^5 \text{ A}$ provides a starting point for further analysis of

the Z-pinch dynamics.

We do the 3D simulation to illustrate this laser induced Z-pinch process. Fig 1 shows the electrons are pulled out by a CP laser in void (negative current represented in blue), while the positive current density are the return current of electrons flowing in the opposite direction (positive current represented in red). The return current density reaches $J = 10^{15} - 10^{16} \text{ A/cm}^2$ (a cross section of $30 \times 30 \text{ nm}^2$, $I_{max} \sim 1.4 \times 10^5 \text{ A}$), consistent with the estimation. Due to the extremely high current density, the induced magnetic field around the nanowire is also significant. The 2d image in Fig. 1 illustrates the transverse magnetic field distribution in the simulation. The maximum field reaches $B_y = 1.0 \times 10^6 \text{ T}$, exceeding the incident laser field ($a_0 = 17$, $B_y = 4.6 \times 10^5 \text{ T}$). This quasi-static magnetic field exerts a $J \times B$ force on both inner and outer current (electrons) of the nanowire. The current on the inner surface of the nanowire is subjected to a force radially inward due to the generated magnetic field, whereas the forces on the outer electrons of the nanowire are opposite in direction. Hence, the nanowire is compressed inward, while electrons extracted from the nanowire are pushed outward.

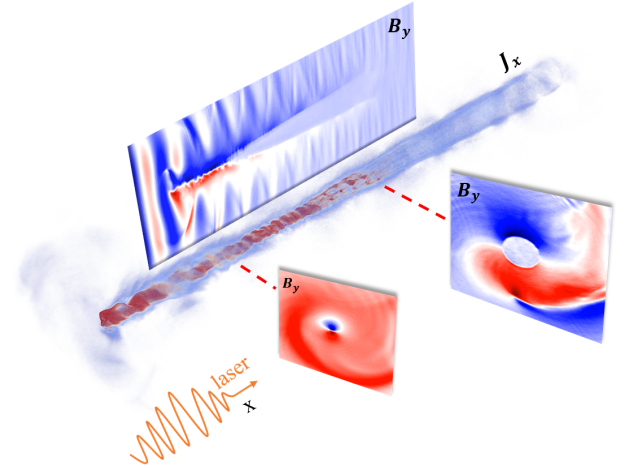


Fig. 1. The 3-D current density and 2-D magnetic fields during the pinch simulation. In the 3D image, the red color represents positive current (max $J_x = 1.4 \times 10^{16} \text{ A/cm}^2$), while the blue color represents negative current. The 2D image illustrates the magnetic field (max $B_y = 1.0 \times 10^6 \text{ T}$). The x-positive direction aligns with the laser propagation and the axial direction of the nanowire, whereas the y and z directions correspond to the radial directions of the nanowire.

When the return electrons are pinched radially inward by Lorentz force, they induce an electric field due to charge separation. Deuterium ions are then drawn and pinched symmetrically inward from the surface by this electric field resulting in the strong radial symmetry for the kinetic energy distribution of deuterium particles within the nanowire. In our following discussion, we estimated that the temperature of deuterium in the Z-pinch is 190 keV by comparing the ratios of nuclear reaction rates. The distribution of momentum on the surface is continuous which like a 2-d shock wave. The mo-

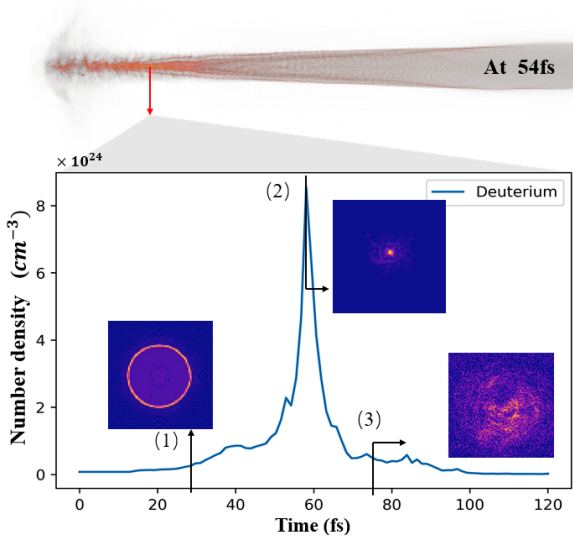


Fig. 2. The spacial and temporal profile of deuterium density. The time-dependent variation of N_{max} is depicted along the curve graph in (a), specifically at the section marked by the red line. Sub-fig(a)(2) demonstrates the particle number density after compression, reaching a value around 10^{25} cm^{-3} .

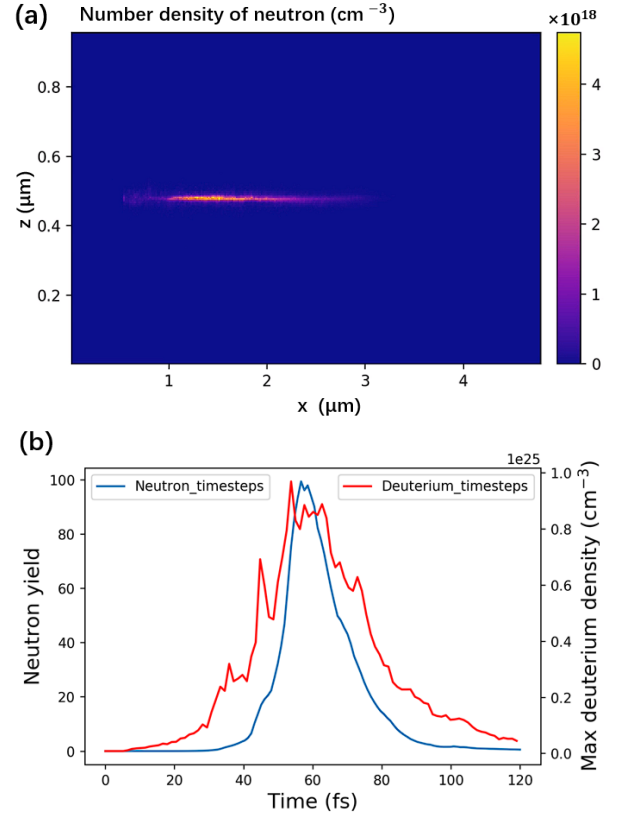


Fig. 3. (a) is Longitudinal cross section of accumulated neutron number density where the blue curve is distribution of neutron along Z-axis, which shows the spacial distribution where D-D nuclear reactions occur. The blue curve in (b) represents the number of nuclear reactions produced per femtosecond, while the red curve depicts the time evolution of deuterium maximum density. The data in the figure has been normalized. Nanowire has a diameter of 300 nm, length of 3.6 μm

146 mentum is between $\pm 50 \text{ MeV/c}$ when deuterium accelerated
 147 to axis center. Those electrons extracted from the nanowire
 148 (that are being pushed outward) will also induce an electric
 149 field, drawing the surface deuterium outward and accelerat-
 150 ing them. If it is an array target, collisions between them are
 151 also significant for nuclear reactions, because of their higher
 152 energy. Eventually the pinched-inward ions are compressed
 153 near the center creating a high density zone (Fig.2). The cor-
 154 responding maximum energy density can reach the order of
 155 $1 \times 10^{24} \text{ MeV/cm}^3$ ($1 \times 10^{12} \text{ J/cm}^3$) at 54 fs, which has two
 156 orders higher than our previous work[30].

157 As shown in Fig. 2, the compression happens within around
 158 $t_c = 10 \text{ fs}$, and the most compression diameter is around
 159 $D = 30 \text{ nm}$. The maximum density of deuterium can exceed
 160 over $\rho_m = 1 \times 10^{25} \text{ cm}^{-3}$, which is 120 times higher than the
 161 initial ion density. The ion (proton or deuterium) radial flux
 162 reaches around $1.0 \times 10^{34} \text{ cm}^{-2} \cdot \text{s}^{-1}$ ($\rho_m \pi D / t_c$). Hence,
 163 nanowires can also serve as other nuclear reaction sources,
 164 such as $p + {}^{11}\text{B} \rightarrow 3\alpha$. These ions concentrate within an ex-
 165 tremely small volume of approximately $30 \times 30 \text{ nm}^2$, causing
 166 intense nuclear reactions, including producing neutrons. For
 167 lasers with $a_0 > 40$, the maximum density in the nanowires
 168 have a slight increase. For example, with $a_0 = 150$, there
 169 will be a maximum density of $1.8 \times 10^{25} \text{ cm}^{-3}$ on the front
 170 of wire, due to an intense axial particle acceleration and the
 171 combined effect of nanowire micro-pinch, which is long be-
 172 fore the peak of laser pulse.

173 When the laser intensity increases, both the magnitude of
 174 the return current density and the maximum ion density rise,
 175 but not indefinitely in our simulation. This would limit the
 176 number of nuclear reactions during the Z-pinch(Fig.4(a)). It
 177 may be caused by stability.

178 Figure 3 demonstrates the number and density of nuclear

179 reactions ($D + D \rightarrow n + {}^3\text{He}$) generated by the Z-pinch.
 180 Here the propagation of the produced neutrons are not consid-
 181 ered. It is the moment when energetic ions are colliding with
 182 each other at the densest vicinity. Due to the extremely high
 183 particle number density, it is seen that nuclear reactions pri-
 184 marily take place around the axis of the nanowire, as shown
 185 in fig 3(a). The neutron density resulting from D-D nuclear
 186 reactions is approximately on the order of 10^{18} cm^{-3} . The ex-
 187 tremely short compression leads to a burst of reactions within
 188 femtoseconds, where reaction rate is over 100/fs at such a
 189 small time scale, as shown in fig 3(b). If suitable nuclear re-
 190 actions are available, the induced reaction shows an ultra-high
 191 peak flux and ultra-short pulse duration. From the simula-
 192 tions, we obtain neutrons with narrow pulse width (30 fs) and
 193 a small source size ($\pi 30 \text{ nm} \times 3000 \text{ nm} = 2.8 \times 10^5 \text{ nm}^2$). The
 194 corresponding neutron (particle) flux may reach $10^{26} \text{ cm}^{-2} \cdot$
 195 s^{-1} .

196 The figure 4(a) illustrates the relationship between laser pa-
 197 rameters (30 fs and 60 fs, circularly polarized and linearly
 198 polarized) with the number of nuclear reactions generated by
 199 the Z-pinch. Additionally, increasing the length is efficient in

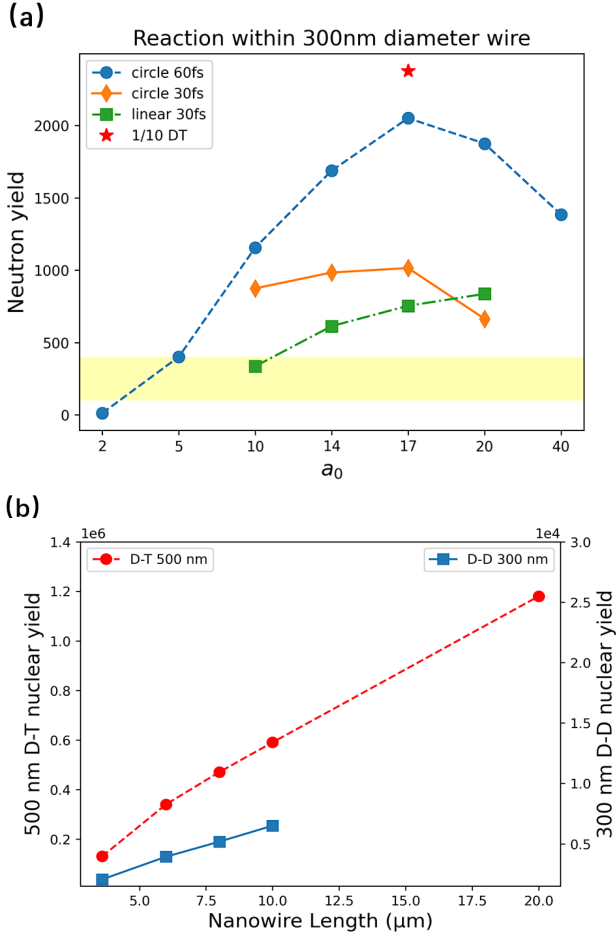


Fig. 4. (a) the relationship between the number of reaction in a nanowire with a diameter of 300 nm, length of $3.6 \mu\text{m}$ and several laser intensity. The blue circle in the diagram represents a 60 fs pulse width circularly polarized laser, while the orange and green marks represent 30 fs pulse width circularly or linearly polarized lasers. The yellow range is the approximate range of nuclear reactions that we estimate can be generated by existing Z-pinch devices under the same substance of material conditions. The red star is one-tenth of D-T reaction counts. (b) number of fusion with various length. The red circle represents D-T fusion and its yield is on the left. The blue square represents D-D fusion and its yield is on the right.

phase. Diameters of nanowires also have an impact on the reaction rates. Under the same conditions, if normalized for substance of material, the efficiency of nuclear reaction generation is the highest in the diameter of 500 nm wire, followed by 300 nm. Both of these efficiencies are higher than those observed in the 200 nm and 800 nm wires.

When the D-T system is considered, the fusion yield is found more than that of D-D by over 10 times. Comparing their yield in the same system, the equivalent temperature [31] at which nuclear reactions occur in this nanowire is around 190 keV. The neutron flux could reach $10^{27} \text{ cm}^{-2} \cdot \text{s}^{-1}$ in the D-T reaction system. For the nanowire with 500 nm diameter, length with $6 \mu\text{m}$, $8 \mu\text{m}$ and $10 \mu\text{m}$ can generate 3.4×10^5 , 4.7×10^5 and 5.9×10^5 neutron, respectively. It is noteworthy that this growth is almost linear with length (Due to the pulse width of the laser, the length needs to be long enough). More than 10^6 neutron could be generated within a single pulse, if the length of nanowire is increased to $20 \mu\text{m}$, as shown in Fig 4(b). Cascade reactions of D-D and D-T also occur within the system.

IV. CONCLUSION

In summary, we first conducted a study on the interaction between lasers and nanowires, with a particular focus on the Z-pinch effect. Notably, the deuterium density within the nanowire could exceed initial density by over a hundred time. We analyze the pinch density and current under different laser and nanowire parameters. It also simultaneously indicates the potential existence of stable regions in the Z-pinch effect induced by lasers. The Z-pinch effect makes laser-driven nanowires a short-time-scale, and high spatial-density environment for nuclear reactions to occur. It's suitable for use as a neutron source, which also possesses the advantages of a small spatial scale ($30 \text{ nm} \times 30 \text{ nm}$), short pulse width 30 fs. This compression leads to an extremely intense and short neutron pulse. Its peak neutron flux reaches $10^{27} \text{ cm}^{-2} \cdot \text{s}^{-1}$. The high-flux nuclear reaction (neutron) sources can be utilized for research in laboratory nuclear astrophysics r-process[32]. The laser can not only pinch the deuterium ions but also for the other particles as sources in nanowires. One typical example is the proton source. With radial flux around $1.0 \times 10^{34} \text{ cm}^{-2} \cdot \text{s}^{-1}$, the proton source will provide a unique way for the two-proton capture reaction during the rp-process[33].

- [1] I. S. Anderson, C. Andreani, J. M. Carpenter, G. Festa, G. Gorini, C.-K. Loong, and R. Senesi, *Physics Reports* **654**, 1 (2016), publisher: Elsevier.
- [2] J. Wei, H. Chen, Y. Chen, Y. Chi, C. Deng, H. Dong, L. Dong, S. Fang, J. Feng, S. Fu, L. He, W. He, Y. Heng, K. Huang, X. Jia, W. Kang, X. Kong, J. Li, T. Liang, G. Lin, Z. Liu, H. Ouyang, Q. Qin, H. Qu, C. Shi, H. Sun, J. Tang, J. Tao, C. Wang, F. Wang, D. Wang, Q. Wang, S. Wang, T. Wei, J. Xi, T. Xu, Z. Xu, W. Yin, X. Yin, J. Zhang,

Z. Zhang, Z. Zhang, M. Zhou, and T. Zhu, *Nuclear Instruments and Methods in Physics Research Section A: Accelerators, Spectrometers, Detectors and Associated Equipment* **600**, 10 (2009).

- [3] R. Garoby, A. Vergara, H. Danared, I. Alonso, E. Bargallo, B. Cheymol, C. Darve, M. Eshraqi, H. Hassanzadegan, A. Jansson, I. Kittelmann, Y. Levinsen, M. Lindroos, C. Martins, Midtun, R. Miyamoto, S. Molloy, D. Phan, A. Ponton, E. Sargsyan, T. Shea, A. Sunesson, L. Tchelidze, C. Thomas,

- M. Jensen, W. Hees, P. Arnold, M. Juni-Ferreira, F. Jensen, A. Lundmark, D. McGinnis, N. Gazis, J. W. II, M. Anthony, E. Pitcher, L. Coney, M. Gohran, J. Haines, R. Linander, D. Lyngh, U. Oden, H. Carling, R. Andersson, S. Birch, J. Cereijo, T. Friedrich, T. Korhonen, E. Laface, M. Mansouri-Sharifabad, A. Monera-Martinez, A. Nordt, D. Paulic, D. Piso, S. Regnell, M. Zaera-Sanz, M. Aberg, K. Breimer, K. Batkov, Y. Lee, L. Zanini, M. Kickulies, Y. Bessler, J. Ringnér, J. Jurns, A. Sadeghzadeh, P. Nilsson, M. Olsson, J.-E. Presteng, H. Carlsson, A. Polato, J. Harborn, K. Sjögreen, G. Muhrer, and F. Sordo, *Physica Scripta* **93**, 014001 (2017).
- [4] J. J. Cowan, C. Sneden, J. E. Lawler, A. Aprahamian, M. Wiescher, K. Langanke, G. Martínez-Pinedo, and F.-K. Thielemann, *Rev. Mod. Phys.* **93**, 015002 (2021).
- [5] F.-K. Thielemann, A. Arcones, R. Käppeli, M. Liebendörfer, T. Rauscher, C. Winteler, C. Fröhlich, I. Dillmann, T. Fischer, G. Martínez-Pinedo, K. Langanke, K. Farouqi, K.-L. Kratz, I. Panov, and I. Korneev, *Progress in Particle and Nuclear Physics* **66**, 346 (2011), particle and Nuclear Astrophysics.
- [6] E. Pian, P. D'Avanzo, S. Benetti, M. Branchesi, E. Brocato, S. Campana, E. Cappellaro, S. Covino, V. D'Elia, J. P. U. Fynbo, F. Getman, G. Ghirlanda, G. Ghisellini, A. Grado, G. Greco, J. Hjorth, C. Kouveliotou, A. Levan, L. Limatola, D. Malesani, P. A. Mazzali, A. Melandri, P. Möller, L. Nicastro, E. Palazzi, S. Piranomonte, A. Rossi, O. S. Salafia, J. Selsing, G. Stratta, M. Tanaka, N. R. Tanvir, L. Tomasella, D. Watson, S. Yang, L. Amati, L. A. Antonelli, S. Ascenzi, M. G. Bernardini, M. Boër, F. Bufano, A. Bulgarelli, M. Capaccioli, P. Casella, A. J. Castro-Tirado, E. Chassande-Mottin, R. Ciolfi, C. M. Copperwheat, M. Dadina, G. De Cesare, A. Di Paola, Y. Z. Fan, B. Gendre, G. Giuffrida, A. Giunta, L. K. Hunt, G. L. Israel, Z.-P. Jin, M. M. Kasliwal, S. Klose, M. Lisi, F. Longo, E. Maiorano, M. Mapelli, N. Masetti, L. Nava, B. Patricelli, D. Perley, A. Pescalli, T. Piran, A. Possenti, L. Pulone, M. Razzano, R. Salvaterra, P. Schipani, M. Spera, A. Stamerra, L. Stella, G. Tagliaferri, V. Testa, E. Troja, M. Turatto, S. D. Vergani, and D. Vergani, *Nature* **551**, 67 (2017).
- [7] J. Alvarez, J. Fernández-Tobias, K. Mima, S. Nakai, S. Kar, Y. Kato, and J. Perlado, *Physics Procedia* **60**, 29 (2014), 3rd International Meeting of the Union for Compact Accelerator-driven Neutron Sources, UCANS III, 31 July–3 August 2012, Bilbao, Spain the 4th International Meeting of the Union for Compact Accelerator-driven Neutron Sources, UCANS IV, 23–27 September 2013, Sapporo, Hokkaido, Japan.
- [8] A. Taylor, M. Dunne, S. Bennington, S. Ansell, I. Gardner, P. Norreys, T. Broome, D. Findlay, and R. Nemes, *Science* **315**, 1092 (2007), <https://www.science.org/doi/pdf/10.1126/science.1127185>.
- [9] X. Jiao, J. Shaw, T. Wang, X. Wang, H. Tsai, P. Poth, I. Pomerantz, L. Labun, T. Toncian, M. Downer, and B. Hegelich, *Matter and Radiation at Extremes* **2**, 296 (2017).
- [10] K. W. D. Ledingham, I. Spencer, T. McCanny, R. P. Singhal, M. I. K. Santala, E. Clark, I. Watts, F. N. Beg, M. Zepf, K. Krushelnick, M. Tatarakis, A. E. Dangor, P. A. Norreys, R. Allott, D. Neely, R. J. Clark, A. C. Machacek, J. S. Wark, A. J. Cresswell, D. C. W. Sanderson, and J. Magill, *Phys. Rev. Lett.* **84**, 899 (2000).
- [11] M. Roth, D. Jung, K. Falk, N. Guler, O. Deppert, M. Devlin, A. Favalli, J. Fernandez, D. Gautier, M. Geissel, R. Haight, C. E. Hamilton, B. M. Hegelich, R. P. Johnson, F. Merrill, G. Schaumann, K. Schoenberg, M. Schollmeier, T. Shimada, T. Taddeucci, J. L. Tybo, F. Wagner, S. A. Wender, C. H. Wilde, and G. A. Wurden, *Phys. Rev. Lett.* **110**, 044802 (2013).
- [12] M. Günther, O. Rosmej, P. Tavana, M. Gyrdymov, A. Skobliakov, A. Kantsyrev, S. Zährter, N. Borisenko, A. Pukhov, and N. Andreev, *Nature Communications* **13**, 170 (2022).
- [13] A. L. Kritcher, C. V. Young, H. F. Robey, C. R. Weber, A. B. Zylstra, O. A. Hurricane, D. A. Callahan, J. E. Ralph, *et al.*, *Nature Physics* **18**, 251.
- [14] W. H. Bennett, *Phys. Rev.* **45**, 890 (1934).
- [15] M. G. Haines, S. V. Lebedev, J. P. Chittenden, F. N. Beg, S. N. Bland, and A. E. Dangor, *Physics of Plasmas* **7**, 1672 (2000).
- [16] M. G. Haines, *Plasma Physics and Controlled Fusion* **53**, 093001 (2011).
- [17] V. Kantsyrev, A. Safronova, A. Esaulov, K. Williamson, I. Shrestha, F. Yilmaz, G. Osborne, M. Weller, N. Ouart, V. Shlyaptseva, L. Rudakov, A. Chuvatin, and A. Velikovich, *High Energy Density Physics* **5**, 115 (2009).
- [18] D. D. Ryutov, M. S. Derzon, and M. K. Matzen, *Rev. Mod. Phys.* **72**, 167 (2000).
- [19] K. K. Ostrikov, F. Beg, and A. Ng, *Reviews of Modern Physics* **88**, 011001 (2016), publisher: American Physical Society.
- [20] V. Kaymak, A. Pukhov, V. N. Shlyaptsev, and J. J. Rocca, *Phys. Rev. Lett.* **117**, 035004 (2016).
- [21] J. J. Rocca, M. G. Capeluto, R. C. Hollinger, S. Wang, Y. Wang, G. R. Kumar, A. D. Lad, A. Pukhov, and V. N. Shlyaptsev, *Optica* **11**, 437 (2024).
- [22] C. Bargsten, R. Hollinger, M. G. Capeluto, V. Kaymak, A. Pukhov, S. Wang, A. Rockwood, Y. Wang, D. Keiss, R. Tommasini, R. London, J. Park, M. Busquet, M. Klapisch, V. N. Shlyaptsev, and J. J. Rocca, *Science Advances* **3**, e1601558 (2017).
- [23] Y. Shou, D. Kong, P. Wang, Z. Mei, Z. Cao, Z. Pan, Y. Li, S. Xu, G. Qi, S. Chen, J. Zhao, Y. Zhao, C. Fu, W. Luo, G. Zhang, X. Yan, and W. Ma, *Optics Express* **29**, 5427 (2021), publisher: Optica Publishing Group.
- [24] A. Curtis, C. Calvi, J. Tinsley, R. Hollinger, V. Kaymak, A. Pukhov, S. Wang, A. Rockwood, Y. Wang, V. N. Shlyaptsev, *et al.*, *Nature communications* **9**, 1077 (2018).
- [25] J. Derouillat, A. Beck, F. Pérez, T. Vinci, M. Chiamello, A. Grassi, M. Flé, G. Bouchard, I. Plotnikov, N. Aunai, J. Dargent, C. Riconda, and M. Grech, *Computer Physics Communications* **222**, 351 (2018).
- [26] D. P. Higginson, A. Link, and A. Schmidt, *Journal of Computational Physics* **388**, 439 (2019).
- [27] D. P. Higginson, I. Holod, and A. Link, *Journal of Computational Physics* **413**, 109450 (2020).
- [28] Z. Zhu, J. Xu, and G.-Q. Zhang, *Physical Review C* **106**, 034604 (2022).
- [29] <https://www.nndc.bnl.gov/> (National Nuclear Data Center).
- [30] D. Kong, G. Zhang, Y. Shou, S. Xu, Z. Mei, Z. Cao, Z. Pan, P. Wang, G. Qi, Y. Lou, Z. Ma, H. Lan, W. Wang, Y. Li, P. Rubovic, M. Veselsky, A. Bonasera, J. Zhao, Y. Geng, Y. Zhao, C. Fu, W. Luo, Y. Ma, X. Yan, and W. Ma, *Matter and Radiation at Extremes* **7**, 064403 (2022).
- [31] W. Bang, M. Barbui, A. Bonasera, G. Dyer, H. J. Quevedo, K. Hagel, K. Schmidt, F. Consoli, R. De Angelis, P. Andreoli, E. Gaul, A. C. Bernstein, M. Donovan, M. Barbarino, S. Kimura, M. Mazzocco, J. Sura, J. B. Natowitz, and T. Ditmire, *Phys. Rev. Lett.* **111**, 055002 (2013).
- [32] J. J. Cowan, C. Sneden, J. E. Lawler, A. Aprahamian, M. Wiescher, K. Langanke, G. Martínez-Pinedo, and F.-K. Thielemann, *Rev. Mod. Phys.* **93**, 015002 (2021).
- [33] H. Schatz, A. Aprahamian, J. Görres, M. Wiescher, T. Rauscher, J. Rembges, F.-K. Thielemann, B. Pfeiffer, P. Möller, K.-L. Kratz, H. Herndl, B. Brown, and H. Rebel,

